EUROFUSION WPS1-PR(16) 15664

B Buttenschoen et al.

Spectroscopic impurity survey in the first operation phase of Wendelstein 7-X

Preprint of Paper to be submitted for publication in
43rd European Physical Society Conference on Plasma Physics (EPS)

This work has been carried out within the framework of the EUROfusion Consortium and has received funding from the Euratom research and training programme 2014-2018 under grant agreement No 633053. The views and opinions expressed herein do not necessarily reflect those of the European Commission.

Spectroscopic impurity survey in the first operation phase of Wendelstein 7-X

B. Buttenschön[1], R. Burhenn[1], M. Kubkowska[2], A. Czarnecka[2], T. Fornal[2], N. Krawczyk[2], D. Zhang[1], N. Pablant[3], A. Langenberg[1], P. Valson[1], H. Thomsen[1], W. Biel[4], J. Aßmann[4], the Wendelstein 7-X team

[1] *Max Planck Institute for Plasma Physics, Wendelsteinstr. 1, 17491 Greifswald, Germany*

[2] *Institute of Plasma Physics and Laser Microfusion, Hery 23 St. 01-497 Warsaw, Poland*

[3] *Princeton Plasma Physics Laboratory, Princeton, NJ, USA*

[4] *Forschungszentrum Jülich GmbH, 52425 Jülich, Germany*

Introduction

During its first operation phase (OP1.1), lasting from December 2015 to March 2016, the optimized stellarator Wendelstein 7-X [1, 2] (W7-X) successfully produced helium and hydrogen plasmas with up to 6 seconds pulse length and up to 4 MJ pulse energy supplied by ECR heating. This operation phase was mainly dedicated to machine commissioning and performance tests, which is why impurity diagnostics monitoring the overall impurity content and evolution within the performed plasma discharges played an important role for the assessment of machine safety.

One of the main tools for overview impurity monitoring is the High Efficiency XUV Overview Spectrometer system (HEXOS), built for W7-X in collaboration with the Forschungszentrum Jülich [3, 4, 5]. Observing the wavelength range $\lambda = (2.5 \ldots 160)$ nm distributed over four spectrometer channels with high spectral and temporal ($f_{\mathrm{spec}} \leq$ 1 kHz) resolution, this instrument covers the most intense resonance lines of intrinsic impurities expected in W7-X plasmas as well as prominent emission lines of injectable tracer impurities (e.g. Ar, Ne, N, but also various solid impurities planned to be injected in the next operation phase). For the larger part of the observed wavelength range, an absolutely cal-

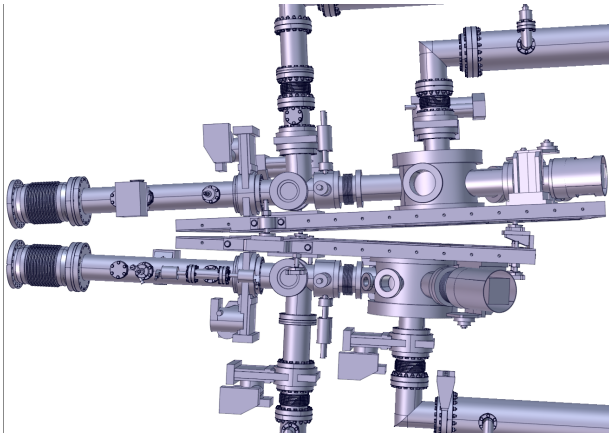

Figure 1: *The HEXOS system consists of four spectral channels, two of which form one double spectrometer. The two double spectrometers are mounted on top of each other with a small angle to have a similar line of sight through the plasma center.*

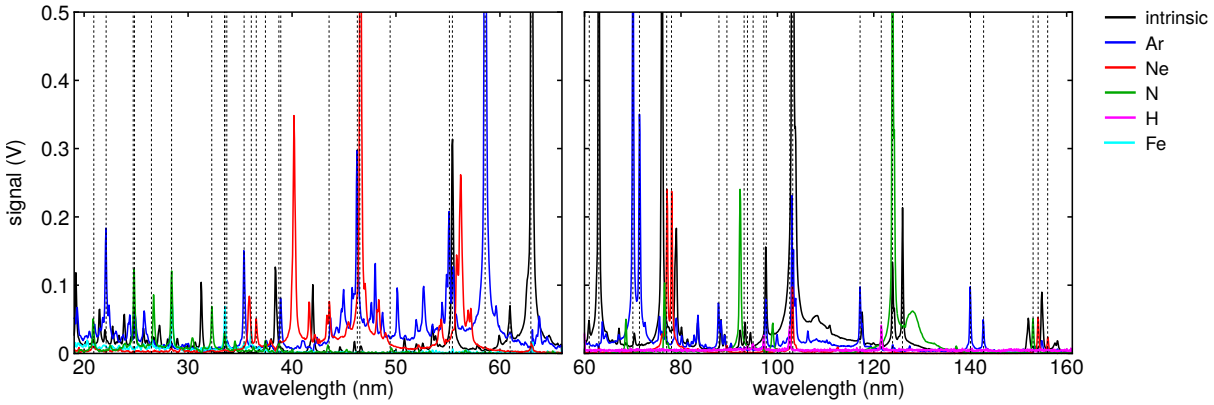

Figure 2: *Spectra of HEXOS channels 3 and 4 used for wavelength calibration. Different colors correspond to different identified impurities. Dashed lines indicate the positions of identifies emission lines.*

ibrated hollow cathode discharge [6, 7] is available as secondary standard source for absolute calibration of the HEXOS system [8].

HEXOS status and calibration during OP1.1

During the first operation phase of W7-X, only two channels of HEXOS were functional, reducing the observable spectral range to $\lambda = (20 \ldots 160)$ nm. The calibration of all channels has still to be performed so that, at present, absolute information about impurity concentrations cannot be derived from the measured spectra. However, a wavelength calibration for line identification could be performed using spectra from W7-X plasmas.

Figure 2 shows six different spectra used for the wavelength calibration of the two available spectral channels together with the location of unambiguously identified emission lines (dashed vertical lines). All spectra are taken from different experiment runs and, in the case of injected impurities (Ar, Ne, N, Fe), are background-corrected with respect to the pre-injection phase spectra. While Ar, Ne and N were injected for diagnostic purposes, the Fe lines are taken from one single event where a small iron flake was released into the plasma. The hydrogen lines are the five brightest Lyman series lines, observed during plasma build-up and in the afterglow. With this calibration covering the entire wavelength region of both spectrometer channels, the average deviation between measured and literature wavelengths $\langle|\lambda_{\mathrm{meas}} - \lambda_{\mathrm{lit}}|\rangle \ll \Delta\lambda$ with the typical line width $\Delta\lambda = 0.13$ nm in spectrometer 3 and $\Delta\lambda = 0.26$ nm in spectrometer 4.

Impurity survey

The overall intrinsic impurity radiation in the observable wavelength range does not vary much between individual experiment programs (see figure 3) and typically consists of oxygen, carbon and nitrogen lines, with several lower intensity emission lines of fluorine, chlorine and sulfur. The presence of S is also confirmed by the X-ray imaging crystal spectrometer (XICS) [9,

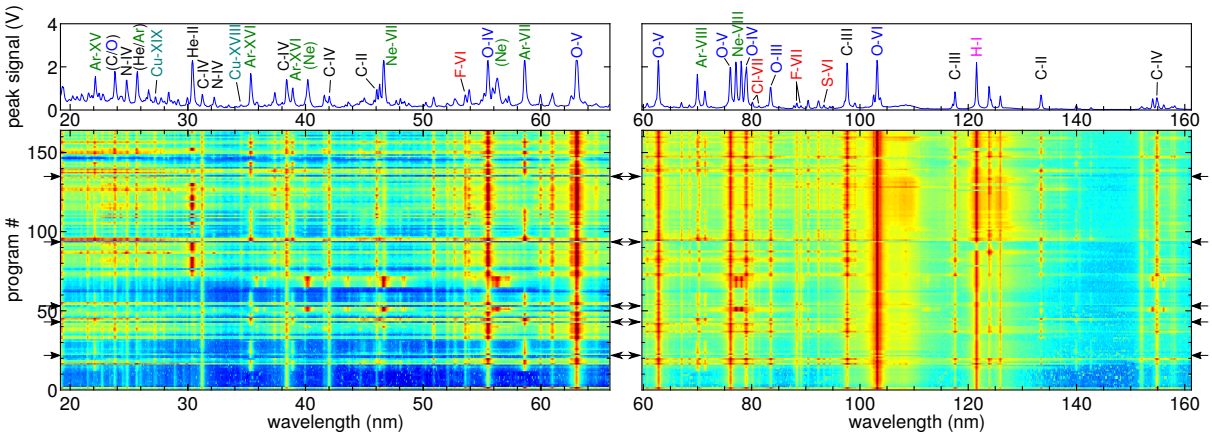

Figure 3: *Overview over all experiments of the last two weeks (in total 6 days) of W7-X operation. Bottom row: average intensity (in a.u.) per wavelength per experiment program; top row: maximum average intensity per wavelength of all programs. Black arrows mark the first experiment of each day.*

10] and the soft X-ray pulse height analysis (PHA) system [11]. The PHA system additionally confirms the presence of Cl in the plasma core. Out of the expected metallic impurities only Cu (Na-like and Mg-like) is consistently visible in HEXOS at very low intensity, while Fe lines occurred only once during the above mentioned iron flake event. Clear deviations from the typical intrinsic impurity composition are obviously found at experiments with diagnostic gas admixtures (see lines of argon, neon and nitrogen) added for diagnostic purposes. The color plots in figure 3 show the average intensity per wavelength and experiment program, where each row is one conducted experiment. The black arrows mark the first experiment of each day, representing the impurity content after glow discharge wall conditioning where the cleanest plasma conditions are expected. The upper plots show the maximum intensities per wavelength over all 163 experiment programs considered here. The most prominent lines are labeled along with some less intense, but constantly visible lines; lines with labels in brackets are two or more lines of the specified elements blending into each other.

Impurity confinement estimation

Using experiment programs with a prefill or injection of Ar as diagnostic gas, a very first estimation about the effective impurity confinement time τ^* (including possible refill of Ar by recycling processes at the vessel wall) can already be made. Figure 4 shows the intensity evolution for different ionization stages of Ar in a discharge with an Ar prefill. While Ar VII to XVI are lines visible in HEXOS, the Ar XVII signal is taken from the XICS system. The decay times τ^* are determined assuming that $I/n_e \propto \exp(-t/\tau^*)$ (with I being normalized to the slightly varying density n_e) for all lines, and measured after the ionization and inwards

transport processes are presumably completed when the temporal behavior should only reflect the confinement of Ar interfering with a certain recycling flux. At this time, the intensities of the Ar VII and Ar VIII lines are already low, but still show a decay significantly slower than that of the higher ionization stages, indicating the presence of a recycling flux. This behavior is comparable for all experiment programs evaluated so far. This analysis, based on only a small number of available experiment programs, determines the effective decay time for Ar as $\tau^* = (150 \ldots 300)$ ms close to the plasma center (i.e., for Ar XV and above), with increasing values of up to $\tau^* \gg 1$ s for the low ionization stages. A more detailed analysis, including different injected gases and the effects of recycling at the plasma boundary, has still to be done.

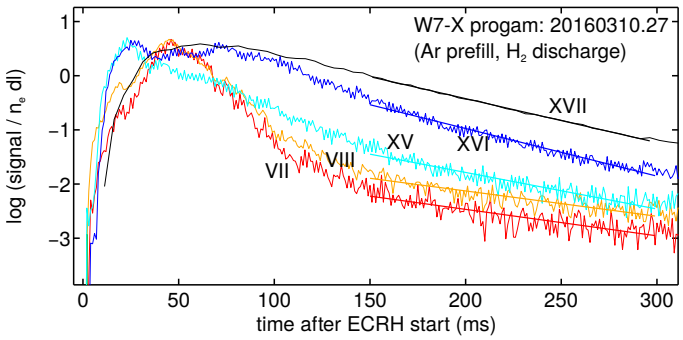

Figure 4: *Traces of Ar lines for one exemplary experiment program with an Ar pre-fill in an H_2 discharge.*

Acknowledgements

This work has been carried out within the framework of the EUROfusion Consortium and has received funding from the Euratom research and training programme 2014-2018 under grant agreement No 633053. The views and opinions expressed herein do not necessarily reflect those of the European Commission.

References

[1] C. Beidler *et al.*, Fusion Technol. **17**, 148 (1990)

[2] H.-S. Bosch *et al.*, Nucl. Fusion **53**, 126001 (2013)

[3] W. Biel, A. Greiche, R. Burhenn, E. Jourdain, D. Lepere, Rev. Sci. Instrum. **75**, 3268 (2004)

[4] W. Biel, G. Bertschinger, R. Burhenn, R. König, E. Jourdain, Rev. Sci. Instrum. **77**, 10F305 (2006)

[5] H. Thomsen *et al.*, J. Inst. **10**, P10015 (2015)

[6] J. Hollandt, M. Kühne, B. Wende, Appl. Opt. **33**, 68 (1994)

[7] J. Hollandt, M. Kühne, M.C.E. Huber, B. Wende, Astron. Astrophys. Suppl. Ser **115**, 561 (1996)

[8] A. Greiche, W. Biel, O. Marchuk, R. Burhenn, Rev. Sci. Instrum. **79**, 093504 (2008)

[9] N.A. Pablant *et al.*, in 41st EPS Conf. on Plasma Phys., P1.076 (2014)

[10] A. Langenberg, J. Svensson, H. Thomsen, O. Marchuk, N.A. Pablant, R. Burhenn, and R.C. Wolf, Fusion Sci. Technol. **69**, 560 (2016)

[11] M. Kubkowska *et al.*, J. Inst. **10**, P10016 (2015)